Title

Endogenous fluorophores enable two-photon imaging of the primate eye.

Journal

Investigative Ophthalmology and Visual Science, 55(7)

Authors

Palczewska, Grazyna
Golczak, Marcin
Williams, David
et al.

Publication Date

2014-06-26

DOI

10.1167/iovs.14-14395

Peer reviewed

Endogenous Fluorophores Enable Two-Photon Imaging of the Primate Eye

Grazyna Palczewska,[1] Marcin Golczak,[2] David R. Williams,[3,4] Jennifer J. Hunter,[3,5,6] and Krzysztof Palczewski[2]

[1]Polgenix, Inc., Cleveland, Ohio, United States
[2]Department of Pharmacology, Case Western Reserve University, Cleveland, Ohio, United States
[3]Center for Visual Science, University of Rochester, Rochester, New York, United States
[4]The Institute of Optics, University of Rochester, Rochester, New York, United States
[5]Flaum Eye Institute, University of Rochester, Rochester, New York, United States
[6]Department of Biomedical Engineering, University of Rochester, Rochester, New York, United States

Correspondence: Krzysztof Palczewski, Department of Pharmacology, Case Western Reserve University, 2109 Adelbert Road, Cleveland, OH 44106-4965, USA; kxp65@case.edu.

Submitted: March 19, 2014
Accepted: June 7, 2014

Citation: Palczewska G, Golczak M, Williams DR, Hunter JJ, Palczewski K. Endogenous fluorophores enable two-photon imaging of the primate eye. *Invest Ophthalmol Vis Sci*. 2014;55:4438–4447. DOI:10.1167/iovs.14-14395

Purpose. Noninvasive two-photon imaging of a living mammalian eye can reveal details of molecular processes in the retina and RPE. Retinyl esters and all-*trans*-retinal condensation products are two types of retinoid fluorophores present in these tissues. We measured the content of these two types of retinoids in monkey and human eyes to validate the potential of two-photon imaging for monitoring retinoid changes in human eyes.

Methods. Two-photon microscopy (TPM) was used to visualize excised retina from monkey eyes. Retinoid composition and content in human and monkey eyes were quantified by HPLC and mass spectrometry (MS).

Results. Clear images of inner and outer segments of rods and cones were obtained in primate eyes at different eccentricities. Fluorescence spectra from outer segments revealed a maximum emission at 480 nm indicative of retinols and their esters. In *cynomolgus* monkey and human retinal extracts, retinyl esters existed predominantly in the 11-*cis* configuration along with notable levels of 11-*cis*-retinol, a characteristic of cone-enriched retinas. Average amounts of di-retinoid-pyridinium-ethanolamine (A2E) in primate and human eyes were 160 and 225 pmol/eye, respectively.

Conclusions. These data show that human retina contains sufficient amounts of retinoids for two-photon excitation imaging. Greater amounts of 11-*cis*-retinyl esters relative to rodent retinas contribute to the fluorescence signal from both monkey and human eyes. These observations indicate that TPM imaging found effective in mice could detect early age- and disease-related changes in human retina.

Keywords: rod photoreceptors, cone photoreceptors, retinoid cycle, two-photon microscopy, primate retina

Imaging of cellular processes at subcellular resolution in vivo is a critically needed approach to understand the origin of pathological processes in living tissues.[1] In many cases, various imaging techniques can provide a superior alternative for evaluating the effects of drug therapy, improving diagnostics, or guiding surgical procedures. One of the emerging visualization techniques is multi-photon (especially two-photon, 2P) excitation fluorescence. Although this is a new imaging modality, the discovery of its underlying physical principles dates back to the development of quantum physics. The theory of 2P absorption was first predicted by Maria Goeppert-Mayer[2] in her 1931 doctoral dissertation, and observed experimentally 30 years later by 2P excited fluorescence of CaF_2:Eu^{2+} crystals.[3,4] Since that time, steady progress in laser and optics technologies has paved the way for practical development of new imaging capabilities that capitalize on 2P absorption.[5]

The eye is an excellent organ for imaging by a multiphoton excitation approach, due to the variable transparency of sclera, cornea, lens, and retina to near infrared (IR) light.[6,7] However, the potential risk of light-induced tissue damage requires minimization of the laser beam energy that could compromise the quality of the imaging signal.[6–9] To overcome this shortcoming, several technical innovations have been introduced. These include adaptive optics used to correct for optical aberrations introduced by the cornea and lens, tunable lasers that deliver pulses shorter than 100 fs in parallel with advanced dispersion compensation, highly sensitive low-noise detectors, and application of sophisticated software algorithms for image alignment, recovery, and correction for body movements (e.g., eye movements, heartbeat, and breathing).[6,7,10] With these advances, it has become feasible to image cellular processes of rod/cone photoreceptor and RPE cells as well as other eye cell types on a routine basis.[6,7,11–19] Of special interest is the study of Hunter et al.,[7] who found that two-photon ophthalmoscopy (2PO) images of the macaque cone mosaic were formed by a signal derived from cone inner segments. Recently, TPM was used to elucidate the flow of molecular events in the retina following light-induced damage to photoreceptor cells in mice.[20]

The eye is also very special for another reason. Our vision depends on vitamin A (all-*trans*-retinol), a fluorescent isoprenoid that is a precursor for many other related chromophores.[21] All-*trans*-retinol and its fatty acid esters are particularly useful for imaging because of their characteristic intrinsic fluorescence.[22] Retinol fluorescence is highly sensitive to solvents. Its quantum yield varies from 0.07 in cyclohexane,[23] 0.027 in hexane,[24,25] 0.016 in 3-methylpentane/triethylamine,[26] and 0.011 in ethanol[27] to 0.015 in isopropanol.[28] This sensitivity to the environment could be very useful when combined with analytical methods to distinguish different biochemical/cellular processes in the retina. Vitamin A is a conjugated polyene compound with several naturally and artificially generated isomers. These isomers are also fluorescent with quantum yields in 3-methylpentane-methylcyclohexane of 0.006 and 0.007 for 9- and 11-*cis* isomers, respectively.[22] Interestingly, in contrast to alcohols, retinal aldehydes exhibit far less fluorescence.[29] Another important group of retinal chromophores are retinal condensation products, which are much more fluorescent than retinols, or any other metabolic product of retinoids.[30] During natural aging, condensation products such as di-retinoid-pyridinium-ethanolamine (A2E) and compounds of similar chemical nature and their oxidized derivatives accumulate within RPE contributing to increased fluorescence of this cell layer.[31,32] Fundus fluorescence of human eye increases significantly with age, has a broad emission between 500 and 750 nm,[33] and resembles A2E fluorescence of human RPE in culture.[34] At 488-nm excitation, Bruch's membrane and sub-RPE deposits in normal eyes exhibited enhanced fluorescence in eyes of donors with AMD.[35] Other all-trans-retinal conjugation products and A2E are considered as biomarkers for elevated levels of potentially toxic retinoids that accelerate the development of retinal degenerative diseases such as Stargardt disease and AMD.[36,37] In more recent studies, Schweitzer et al.[38] used time-resolved autofluorescence measurements recorded simultaneously in 16 spectral channels (445–605 nm) on fundus samples from a donor with significant extramacular drusen. These authors detected a bright fluorescence from RPE lipofuscin with a maximum at 510 nm and a lifetime of 385 ps. This fluorescence declined at longer wavelengths but was still substantial at 600 nm. These investigators also characterized different types of drusen[39]; most that did not contain lipofuscin and exhibited fluorescence with a maximum at 470 nm and lifetime of 1785 ps. Other researchers have observed the absence of elevated levels of A2E in the macula.[31,40] It was also proposed that A2E and other precursors of lipofuscin have a photoreceptor-derived origin as a result of continuous transport of free 11-*cis*-retinal to visual pigments.[41] However, recent imaging of retinal degeneration after an intense bleach in a Stargardt disease–mouse model clearly demonstrated that condensation products are formed in photoreceptors, but only as a result of rhodopsin bleaching and not 11-*cis*-retinal transport.[20] These aberrant fluorophores, that exhibit different spectral characteristics than retinols, are also readily detectible by 2PO imaging with a new class of femtosecond pulsed lasers with an extended tuning range.[9] Both NADH and NADPH display fluorescent spectral properties similar to retinoids,[42,43] and can contribute to the fluorescence signal in native tissue.[11] Thus, vitamin A–derived retinoids and dinucleotides are natural fluorophores with absorption spectra that respond to multiphoton excitation, bypassing the filter-like properties of the cornea and lens.

In recent years, we took advantage of 2PO to visualize cellular structures successfully in the eyes of mouse models in vitro and in vivo. These studies revealed previously unknown molecular processes that accompany visual chromophore regeneration and the pathology of light-induced retinal damage.[44] However, the real question is if these processes occur in human eyes and whether TPM can be used to diagnose human retinal pathology. Therefore, the next logical step is to develop the knowledge and instrumentation that will allow imaging primate and human retinal tissue. However, anatomical differences as well as disparities in retinal organization and retinoid composition observed between murine and human eye could constitute major challenges in achieving this goal. Here, we report the molecular components responsible for the endogenous fluorescence signal and provide 2PO images of monkey retina, the closest surrogate to human retina that disclose discrete features of cone cell organization in the macula region.

Methods

Animals

All animal procedures and experiments were approved by Case Western Reserve University and conformed to recommendations of the Association of Research for Vision and Ophthalmology. Freshly enucleated eyes of *cynomolgus* monkey (*Macaca fascicularis)* were obtained from Ricerca Biosciences (Painesville, OH, USA).

Human Eyes

Deidentified human eyes were obtained from the Cleveland Eye Bank (CEB) following a preapproved protocol. Only eyes from individuals who had no known eye disease were employed for the experiments described below. We coordinated closely with the CEB to reduce the time between death and tissue availability for experimentation. Eyes scheduled for HPLC and MS analyses were placed at −80°C within 9 hours post mortem.

Retinal Tissue Preparation for TPM Imaging

Six freshly enucleated eyes from a 4-year-old *cynomolgus* monkeys (*Macaca fascicularis)* were obtained from Ricerca Biosciences. Immediately after enucleation, eyes were placed in a 0°C 1 × PBS solution composed of 9.5 mM sodium phosphate, 137 mM NaCl, and 2.7 mM KCl, pH 7.4. To obtain clean cuts before dissection, each whole eyeball was submerged for 10 minutes in a room temperature fixative prepared by mixing 20 mL of 10% paraformaldehyde with 25 mL of deionized water and 5 mL of 10 × PBS (95 mM sodium phosphate, 1.37 mM NaCl, and 27 mM KCl, pH 7.4) to get a total of 50 mL. After detaching the cornea and lens, the vitreous was carefully removed and the eye cup was cut into four clover leaf-shaped portions. When needed, the retina was gently lifted from the RPE. For imaging of fixed retina, a secondary 10- to 20-minute fixation step was applied with the solution described above. Before imaging, the retina was placed on filter paper and transferred onto the bottom of a glass-bottom dish (MatTek Corp., Ashland, MA, USA) with a minimal volume of PBS. A small piece of folded aluminum foil was placed on top of the filter paper to keep the retina submerged and in contact with the glass.

2PO Imaging

To obtain images formed by intrinsic fluorophores present in retinal neuronal cells, we used a laser scanning confocal microscope (Leica TCS SP2 or Leica TCS SP5; Leica Microsystems, Inc., Wetzlar Germany) each equipped with an inverted stand (Leica MIRE2; Leica Microsystems, Inc.); a fs laser (Chameleon; Coherent, Inc., Santa Clara, CA, USA)

delivering 140 fs pulses at 730 nm; a band-pass filter HQ 465/160 (Chroma Technology, Corp., Bellows Falls, VT, USA); and a photomultiplier tube detector in a nondescanned configuration. Laser light was focused on the sample with a HCX PL APO CS 40.0 × 1.25 oil objective and the induced fluorescence was collected by the same lens after separating the excitation light with a dichroic mirror. For imaging photoreceptors, light entered the retina from its outer segment side, and for imaging the ganglion cell layer, light entered the sample from the nerve fiber layer side. Spectral characterization was performed without a dichroic mirror or band-pass filter. Spectral data were obtained with internal detectors (Leica Microsystems, Inc.) in the descanned configuration. In this setup, light emitted from the sample was collected by the photomultiplier tube detector after passing through a prism which split the light into a spectrum ranging from 400 to 750 nm. Fluorescence of the acquired raw images was quantified by statistical analyses with commercial confocal software (Leica Confocal Software version 2.6. SigmaPlot; Systat Software, San Jose, CA, USA).

Analysis of Retinoid Composition in Human and Monkey Eye

All procedures involving eye handling and retinoid extraction were done under dim red light. Immediately before HPLC analyses, eyes were thawed on wet ice and the cornea, lens and vitreous were removed, leaving the remaining eye cup intact for visual inspection before biopsies were taken in the central and peripheral parts of the RPE/retina. Retina and RPE were combined to obtain accurate quantification of retinoids. Macular tissue was excised with a 5-mm circular trephine centered on the fovea. Temporal, nasal, inferior, and superior regions of retinal and RPE tissues were excised with the trephine centered at least 10 mm from the fovea and the nearest edge of a neighboring punch. The sample was briefly sonicated and homogenized in 5 mL of 67 mM phosphate buffer, pH 7.4, in 50% methanol (vol/vol) and then divided into two equal portions. Hydrophobic retinoids were extracted with 4 mL of hexane following a 20-minute incubation with 40 mM hydroxylamine at room temperature, whereas retinal conjugates, including A2E, were extracted twice with 4 mL of chloroform. For MS-based quantification, the homogenate was supplemented with 500 pmol of deuterated A2E (10D-A2E) as an internal standard, prior to organic solvent extraction. To facilitate efficient phase separation, samples were centrifuged at 10,000*g* for 10 minutes. Organic solvents were collected and subsequently dried down in a vacuum concentrator (SpeedVac; Thermo Fisher Scientific, Inc., Waltham, MA, USA). Prior to HPLC separation, samples were redissolved in 400 μL of hexane (for nonpolar retinoids) or acetonitrile (for A2E analyses). Retinyl esters, retinal oximes, and retinols were separated on a normal phase silica column (Agilent-Si, 5 μm, 4.6 × 250 mm; Agilent Technologies, Santa Clara, CA, USA) in a stepwise gradient of ethyl acetate in hexane (0.5% for 15 minutes, 6% up to 60 minutes) at a flow rate of 1.4 mL/minute. Separation of retinoids was monitored by their absorbance at 325 nm. Individual compounds were identified by their characteristic UV/Vis spectra and quantified based on standard curves obtained for the corresponding synthetic standards. For A2E analysis, the organic extract was injected onto a C18 reverse-phase HPLC column (5 μm, 250 × 4.6; Phenomenex, Torrance, CA, USA) and analyzed in a linear gradient of acetonitrile/isopropanol (50%, vol/vol) in water from 80% to 100%. All solvents contained 0.1% formic acid (vol/vol). The gradient was developed over 30 minutes at flow rate of 1 mL/minute. MS-based detection and quantification of A2E was performed with an LXQ linear ion trap mass spectrometer (Thermo Fisher Scientific, Inc.) equipped with an atmospheric pressure chemical ionization source. Parameters of ionization and detection were optimized with a synthetic A2E standard to achieve the highest possible sensitivity. Levels of A2E in the analyzed samples were quantified based on the linear relationship between the ion intensity peak area corresponding to A2E and the corresponding deuterated internal standard.

Results

Characterization of Photoreceptor Cells in Fresh Primate Retina

To characterize photoreceptor cells in primate eye, we first compared two-photon microscopy images of fresh (Fig. 1A) and fixed (Fig. 1B) retina at different *z*-axis (the long axis of photoreceptor cells) locations. Both fixed and unfixed retina displayed similar features, including the level of fluorescence and arrangement of photoreceptors. Notable characteristics were: (1) the tips of fluorescent portions of cone outer segments were smaller in diameter than rod outer segments; (2) cone outer segments were surrounded by a 2- to 5-μm wide ring of nonfluorescent matrix; (3) the diameter of rod cells was virtually unchanged between the inner and outer segments; and (4) cone inner segments evidenced a markedly increased diameter of up to 6 μm more than that of the outer segments. One major difference between the two preparations was that photoreceptors in unfixed retina were bent by contacting the coverslip glass during imaging with an inverted microscope. Additionally, fixed photoreceptors were slightly more rigid which allowed us to obtain crisp *z*-axis sections of individual photoreceptors (Fig. 1B).

Visualization of Ganglion Cell Layer

To image the ganglion cell layer without any staining or extrinsic fluorophores, we relied on the contrast between the nuclei which are free of fluorophores and the brighter cell bodies (Fig. 2). The first TPM *z*-axis section shows the arrangement of the nerve fiber layer (Fig. 2A). Consecutive sections along the z-axis (Figs. 2A–F) show individual cells in the ganglion cell layer coming in and out of focus.

Fluorescence of Inner and Outer Segments

Brighter cone inner segments were clearly defined against the darker rod inner segments at deeper depths, reaching a maximum brightness at 50 to 60 μm away from the tips of rod outer segments (Figs. 3A, 3B). Fluorescence spectra from outer and inner segments (Fig. 3C) nearly overlapped showing maxima at 480 nm characteristic of retinol and its esters. The small shoulder seen in the inner segment spectrum with a maximum at 456 nm could indicate a contribution of NAD(P)H to the fluorescence signal.[45] Cone to cone spacing was measured at 1, 6, and 10 mm away from the fovea and corresponded to distances of 7.4 ± 0.5 μm, 12.8 ± 2 μm, and 18.3 ± 3 μm, respectively (Fig. 4), in agreement with a previous report.[46] Interestingly, after prolonged TPM imaging, photoreceptors exposed to imaging light exhibited greater fluorescence of their inner segments (Fig. 5A). This contrasts with the typically observed fluorophore bleaching and accompanying reduction in fluorescence when imaging retinal sections. However, it is consistent with the previously observed increase in fluorescence emission in response to bleaching of photoreceptors in the eye of a living primate.[7]

Investigative Ophthalmology & Visual Science

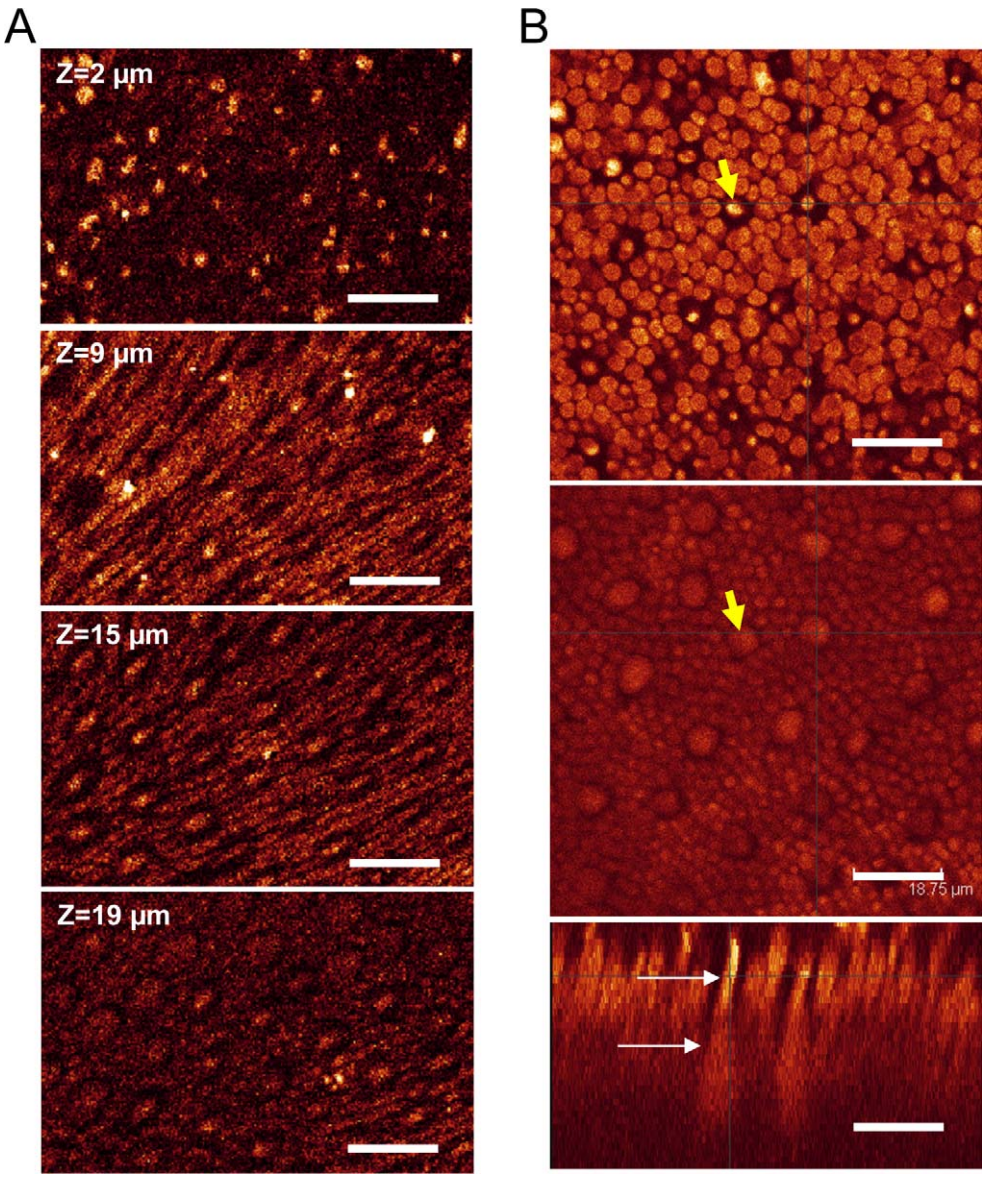

Figure 1. Intrinsic fluorophores in 4-year-old *cynomolgus* monkey retina allow visualization of rod and cone photoreceptors by TPM. (**A**) Two-photon microscopy images of fresh, unfixed retina, taken at different *z*-axis locations. The *z*-axis locations relative to the tips of outer segments are indicated in each image; the top image was 2 µm away from the tips of the outer segments, whereas the bottom image was 19 µm away from the tips of the outer segments. (**B**) En face images of fixed retina taken at *z*–axis locations indicated with *white arrows* in the *bottom panel* are shown in two *upper panels*. A *yellow arrow* points to an outer segment in the *upper panel* (see *upper white arrow* in *bottom panel*) and to the inner segment of the same photoreceptor in the *middle panel*. A *z*-axis section assembled from the series of *z*-stack images is shown in the bottom panel. Two *white arrows* point to the same cone cell as the *yellow arrows* in the *right upper* and *middle* panels. *Scale bars*: 19 µm.

Notably, this increase was more pronounced in cone compared with rod inner segments (Fig. 5B).

Intrinsic Fluorophores Present in Human and Monkey Retina

Noninvasive visualization of retina by 2PO depends on natural fluorophores present in photoreceptor and RPE cells. To provide an analytical evaluation of these compounds in monkey and human eye, we determined the composition of retinoid- and nicotinamide adenine dinucleotide-based chromophores in their corresponding retina extracts.

Aside from readily detectable retinals, HPLC separation of vitamin A metabolites extracted from monkey and human eyes revealed a major pool of retinyl esters predominantly in the 11-*cis* configuration along with noticeable levels of 11-*cis*-retinol characteristic of cone-dominant retinas and retinas that contain cone-enriched regions (Figs. 6A–C). Distribution of these vitamin A metabolites within the retina was not uniform. The macula region exhibited a much higher amount of all of the quantified retinoids than peripheral regions of the retina (Fig. 6C). Levels of 11-*cis* and all-*trans*-retinals were elevated up to 6-fold, whereas the amount of fluorescent retinyl esters was 2 times higher. In addition to the components of the visual cycle, these eyes contained high levels of retinal condensation products. The average amount of A2E quantified in six monkey samples was 160 pmol/eye, comparable with values obtained for human tissue (Figs. 6D, 6E).[47]

Aside from retinoid-based chromophores, other major components that contribute to cell autofluorescence are

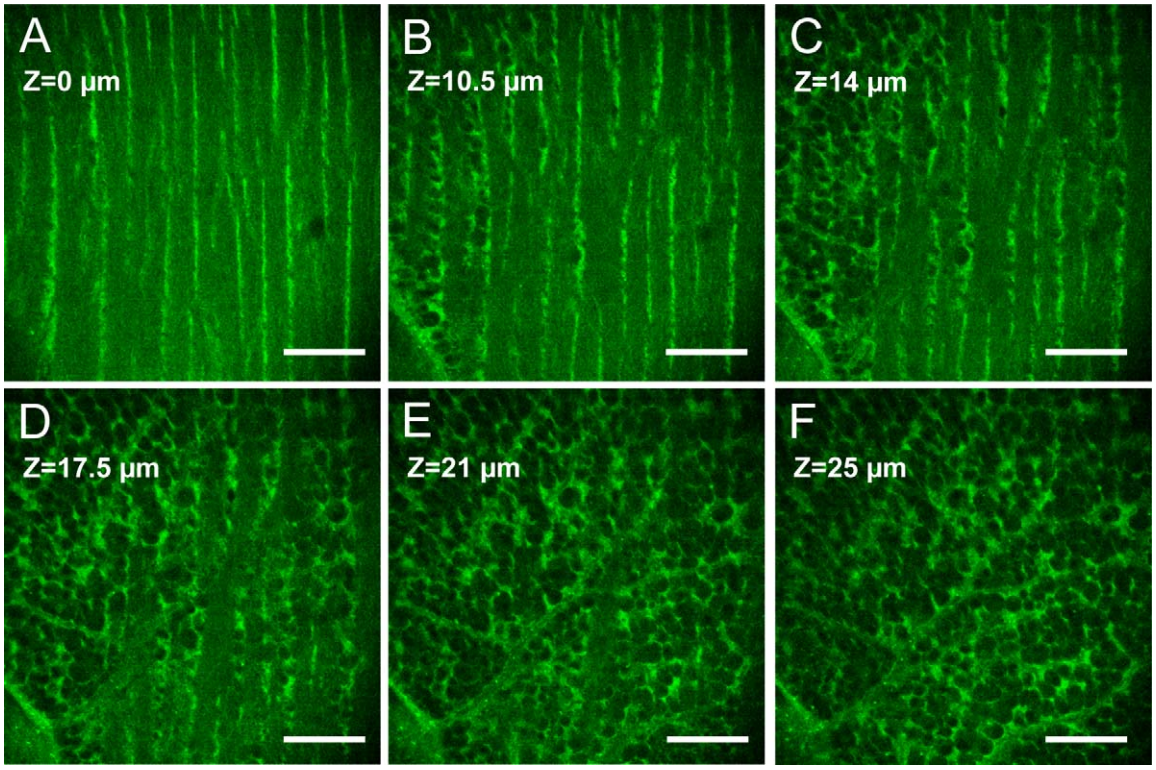

Figure 2. Two-photon microscopy XY sections of 4-year-old *cynomolgus* monkey retinal tissues along the eye optical axis (*z*-axis). The nerve fiber layer (**A**) is at the arbitrary *z*-axis location equal to 0 μm and the ganglion cell layer (**F**) is at 25 μm; *z*-axis locations of (**B**), (**C**), (**D**), and (**E**) are: 10.5, 14, 17.5, and 21 μm, respectively. Depth indications and *scale bars* representing 20 μm are included in each panel.

NADH and NADPH excited in the 320 to 360 nm range. To estimate the potential contribution of nicotinamide adenine dinucleotides to the fluorescence signal, we assessed the levels of these coenzymes in monkey retina extracts by using LC/MS. Although we found 3 nmols of NAD^+ per retina on average in the tested samples, we could not detect either of its reduced forms, NADH or NADPH. This result could be explained by a natural excess of NAD^+ over NADH or NADPH and/or a selective oxidative environment of the cell extracts that facilitated a decrease in NADH concentration.

Discussion

Infrared excitation light that nondestructively penetrates deep into tissues while maintaining a tightly focused laser beam enables imaging the cellular organization of the retina in fine detail. In this report, we show that naturally fluorescent retinoids provide sufficient contrast to discriminate anatomical features of the primate eye. A series of TPM images taken of fresh, unfixed retina along the *z*-axis revealed the structures of inner and outer segments of both rods and cones which could be well discriminated from each other by their difference in size. Moreover, an entire cone could be visualized (Fig. 1). Considering the absorption and scattering of both excitation and fluorescence light, one might expect in our imaging configuration a decrease in the detected fluorescent signal of inner versus outer segments. Though, we observed this trend for rod photoreceptor cells, it was reversed in some cone cells. Even though we could see bright fluorescence from cone outer segments, the fluorescence from cone inner segments was even further increased. Although our results confirmed previously reported increased fluorescence of the inner segments in dissected primate retina,[7] the fluorescence from outer segments was much greater in our experimental setup. This difference could result from differences in the light pathway. In contrast to the previous study where light entered retina from the ganglion cell layer, in our experimental setup light penetrated the retina from the photoreceptor side, without obstruction from other retinal layers. Another contributing factor might be that in the previous study, photoreceptors were attached to the RPE, which provides a metabolic clearance path for all-*trans*-retinol.[21] In agreement with our results, the relatively uniform fluorescence along the inner and outer segments was previously observed in isolated mouse rod cells.[48]

The fluorescence spectra from photoreceptor cells exhibited a maximum around 480 nm indicative of all-*trans*-retinol. However, the relatively broad maximum suggested the presence of multiple fluorophores that contributed to this fluorescence which was further indicated by the slight shoulder around 456 nm in the emission spectra (Fig. 3C). The highest amount of retinoids was found in the central region (Fig. 6C). This observation correlates with the highest RPE65 activity and the protein levels needed for production of 11-*cis*-isomers that were seen in the central part of the macaque eye.[49] Especially prominent were 11-*cis*-retinyl esters. Neither of these 11-*cis* chromophores are abundant in mouse eyes; however, they contribute to the fluorescence signal from monkey and human retinas.[50,51] Adding both *cis* and *trans* isomers we had on average ~4 pmol per mm^2 of retinal area. This compares well with previously reported ~4 pmol per mm^2 of retinal area content of retinyl esters in WT mice.[52] Altogether, the current data are consistent with high levels of 11-*cis*-retinyl esters observed in cone-dominant retinas and in retinas that contain cone-enriched regions.[53,54] It should be noted that the total amount of retinoids found in the human eye qualitatively agrees with previous measurements of

Investigative Ophthalmology & Visual Science

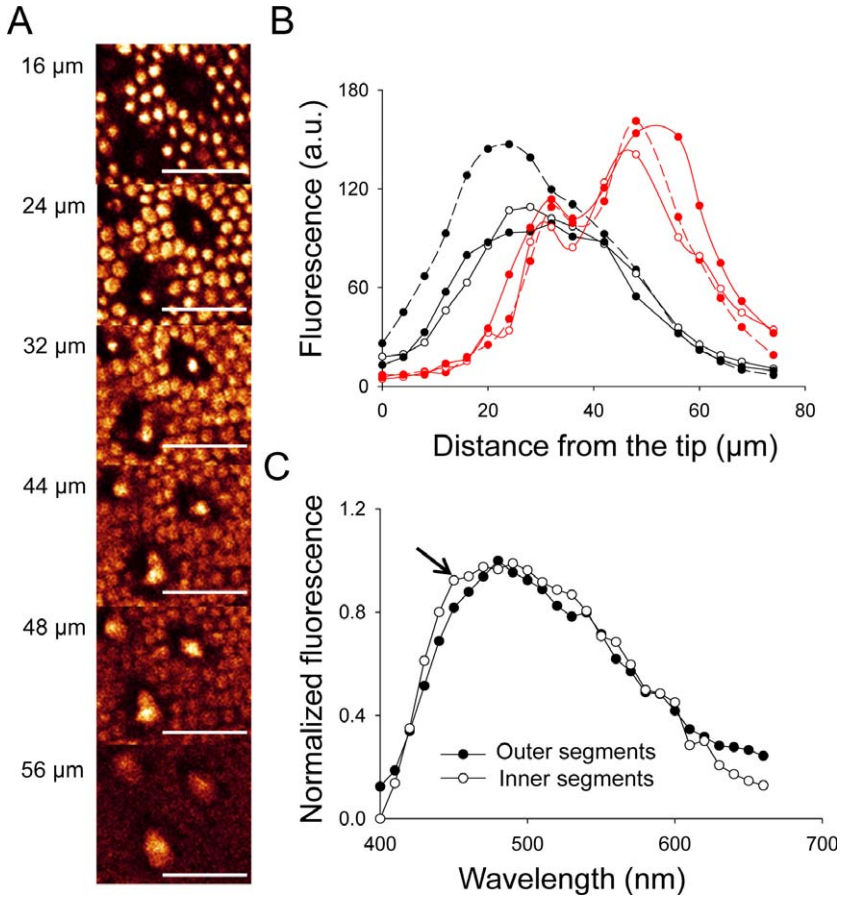

Figure 3. Changes in 2PO induced fluorescence along the outer and inner segments of 4-year-old *cynomolgus* monkey retinas. (**A**) Two-photon microscopy XY sections at *z*-axis locations indicated next to the images. *Scale bars*: 20 µm. (**B**) Mean pixel values for three cones (*red*) and three rods (*black*) along the *z*-axis from the tip of the outer segment (distance = 0), toward the inner nuclear layer. (**C**) Fluorescence spectra from outer segments (*black circles*) and inner segments (*white circles*). The fluorescence from inner segments is shifted toward a shorter wavelength, with a shoulder (*arrow*) at 456 nm indicative of a plausible NADPH contribution.[45]

retinoids in 28 donor human eyes.[55] Approximately half of these retinoids were in the form of retinyl esters and half as postmortem bleached all-*trans* and unbleached 11-*cis*-retinal (Fig. 6C).[55] The average amount of A2E found in primate eye was ~0.2 pmol per mm^2 of retinal area, comparable with previously reported ~0.3 pmol per mm^2 of retinal area in 6-month-old WT mice.[56]

Although we could not detect significant levels of NAD(P)H, its contribution to the overall fluorescence signal cannot be excluded. Emission fluorescence spectra of these dinucleotides are comparable with those of retinoids,[57] and because these water soluble compounds reside in an aqueous phase, their fluorescence is more susceptible to quenching than that of membrane-bound retinoids. Moreover, NAD(P)H levels decline

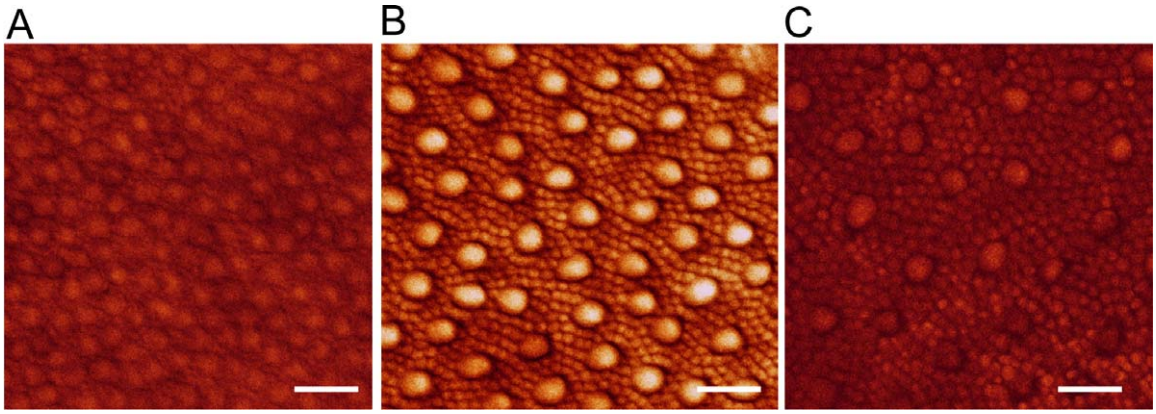

Figure 4. Comparison of TPM images of the inner segment layer at different distances from the fovea in 4-year-old *cynomolgus* monkey retina. Cone-to-cone distances were calculated to be: at 1 mm (**A**), 7.4 ± 0.5 µm; at 6 mm (**B**), 12.8 ± 2 µm; and at 10 mm (**C**), 18.3 ± 3 µm. *Scale bars*: 15 µm.

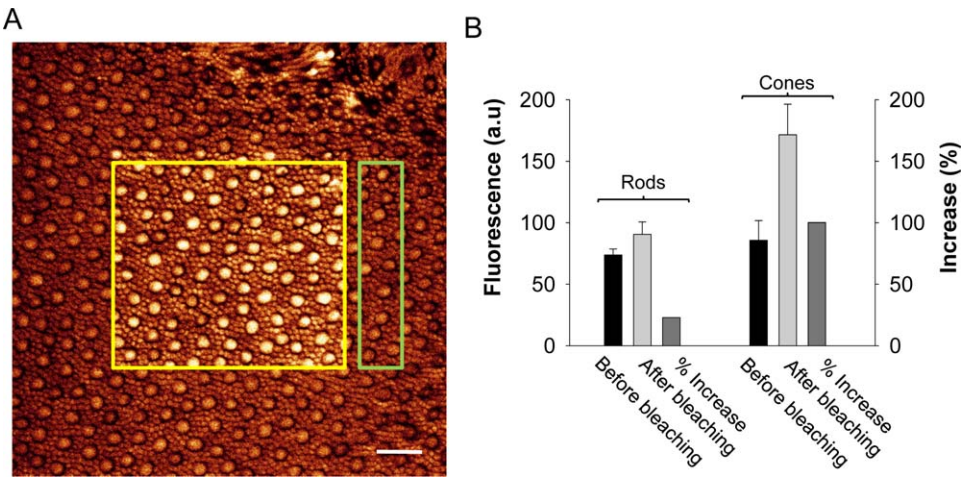

Figure 5. Fluorescence from the inner segments of a 4-year-old *cynomolgus* monkey retina is increased after prolonged TPM imaging. (**A**) Two-photon microscopy image of inner segments. The *center square* shows the increased fluorescence of an area outlined in *yellow* that was exposed to (bleached by) IR light at 730 nm. This fluorescence was on average 53% greater than in the peripheral region outlined in green that was not exposed to the IR light. *Scale bar*: 20 μm. (**B**) Plots of mean fluorescence of rods and cones before and after bleaching with the IR light.

rapidly in isolated tissues to those below detection.[58] Even though we did not detect significant levels of NAD(P)H in examined retinal extracts, a contribution of NAD(P)H to the recorded fluorescence cannot be totally excluded. These conclusions are consistent with the substantially reduced fluorescence in mouse eyes lacking retinoids (lecithin-retinol acyl transferase knockout mice).[9,10,20,44] Thus, retinoids (retinol and esters, and condensation products of retinal) are the main fluorophores of the eye and the contributions from NADPH (NADH) or flavonoid adenine dinucleotides ($FADH_2$) are much lower.

Infrared light also provided images of the ganglion cell and nerve fiber layers (Fig. 2) obtained through the nerve fiber layer and without any exogenous staining. In previous work, we had shown two-photon images of photoreceptors obtained through the anterior segment.[7] Together, these findings indicate the possibility that this modality could be useful in counting ganglion cells during the progression of glaucoma. Such noninvasive techniques could have a tremendous impact on testing and developing the next generation of antiglaucoma drugs. However, these images are currently less bright than those obtained from imaging of photoreceptors/RPE and the identities of the endogenous fluorophores are yet unknown.

Rods and cones are unevenly distributed in the primate eye with the highest concentration of cones in the fovea.[59] Two-photon microscopy can be used to map these differences in cone cell distribution within retina. Figure 4 demonstrates that imaging different sectors of the retina can provide information about the local density and health of these cells as it relates, for example, to the aging process and AMD. However, this analysis should be done in parallel with that of rods because rods are affected earliest in both aging and AMD.[60–63]

The increase in fluorescence emission from the retina in living primate eye after bleaching with IR light was previously observed.[7] Furthermore, this increased emission originated from the inner segments. Here, we also observed that fluorescence in the area exposed to IR light at 730 nm for a prolonged period was on average 53% greater than in the region unexposed to this light (Fig. 5). These results indicate that at least photoisomerization of visual pigments, the first step of the retinoid cycle, still took place in our retinal preparation, and that 730-nm light can bleach both cone and rod pigments.

Visualization of dynamic changes in photoreceptor fluorescence, in response to illumination and the previously reported capability to identify retinosomes and condensation products in RPE,[9,10] indicate that TPM imaging has the potential to detect and monitor early molecular changes caused by AMD and defects in retinoid metabolism. Recently, among different types of drusen,[64] the presence of reticular pseudodrusen (also called reticular drusen) appear to most closely correlate with the progression toward AMD. In one recent study, 40 out of 118 eyes of patients with reticular pseudodrusen progressed to late AMD.[65] These subretinal deposits also were associated with a decrease in choroidal thickness and shortened photoreceptor cells.[66,67] Two-photon microscopy, with its characteristic high resolution in the *z*-axis (along photoreceptors), use of tunable lasers, and the capability to differentiate among different intrinsic fluorophores, offers a methodology to learn about reticular pseudodrusen. Thus, TPM can be used to analyze reticular pseudodrusen formation at the earliest stages, differentiate among different types, pinpoint their exact locations, and provide information about their spectral properties. Indeed, all the above indicate the capability of TPM to assess the efficacy of pharmacological treatments for various malfunctions of retinoid metabolism as well as the progression of retinal degeneration. The application of multiphoton excitation (MPE) not only complements, but far exceeds the capabilities of optical coherence tomography (OCT) or scanning laser ophthalmoscopy. Multiphoton excitation can image fluorophores at wavelengths not accessible by these more conventional eye imaging techniques. Thus, MPE imaging can detect and quantify retinoids involved in the visual cycle and their potentially toxic condensation products, making it the best current method to follow progression of retinal pathology in a non-invasive and reproducible manner. These capabilities also make TPM a very exciting tool for the development of new therapeutics, because it can dramatically shorten the time needed to follow the progression of retinal disorders, both in animal models and humans.

It is becoming increasingly clear that formation of reticular pseudodrusen is closely correlated with clinical progression toward AMD.[68–70] Knowledge about the molecular basis of their formation is scant, but essential for the development of rational drug therapies. Improved imaging techniques are needed to increase the rate of discovery, and 2PO imaging could be such a key imaging procedure. Perhaps the most

Investigative Ophthalmology & Visual Science

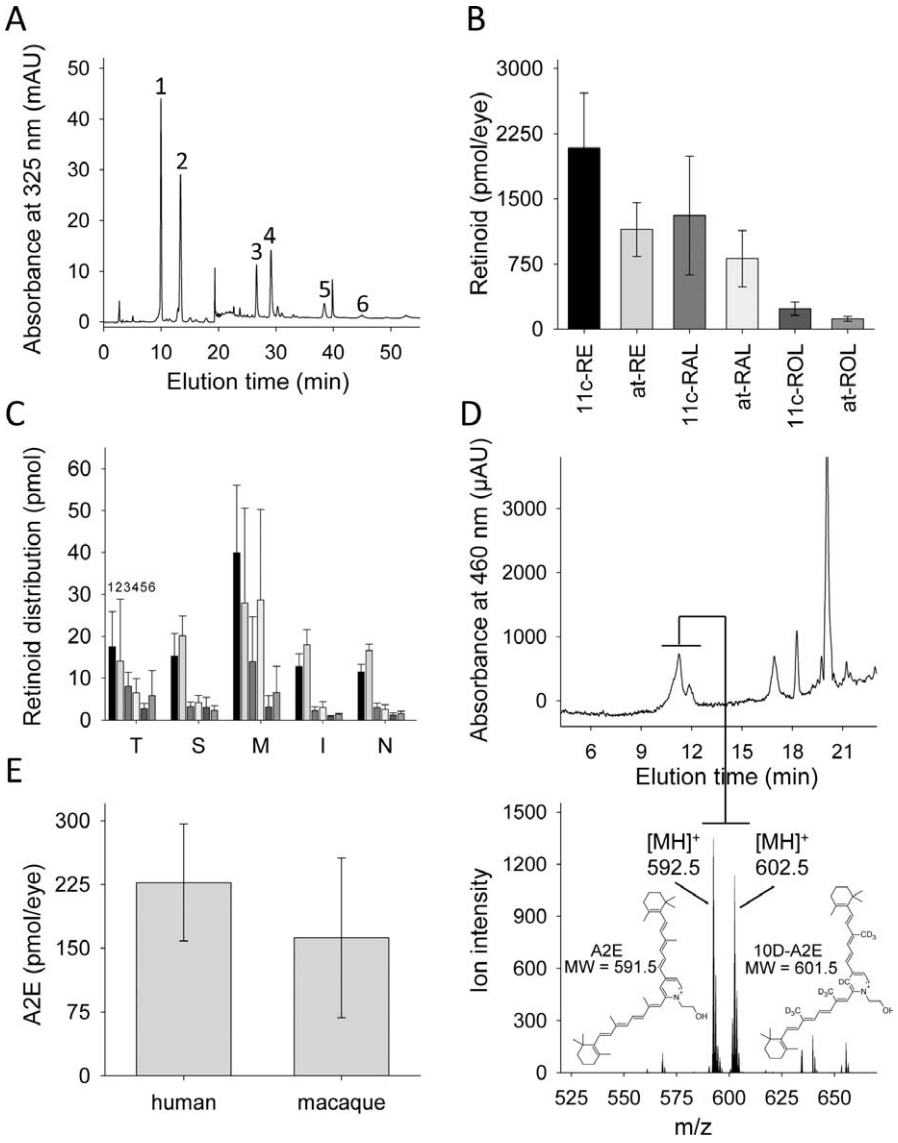

Figure 6. Retinoid composition and distribution in human and monkey eyes. (**A**) High-performance liquid chromatogram showing representative separation of retinoids extracted from macaque eye. The labeled chromatographic peaks correspond to: (1) 11-*cis*-retinyl esters; (2) all-*trans*-retinyl esters; (3) 11-*cis*-retinal oxime (*syn*); (4) all-*trans*-retinal oxime (*syn*); (5) 11-*cis*-retinol; and (6) all-*trans*-retinol. (**B**) Quantification of the main retinoids in 4-year-old *cynomolgus* monkey eyes ($n = 6$). *Bars* represent SDs of the mean. (**C**) Retinoid distribution in human eyes ($n = 4$). Regions of the eye (retina/RPE punches) are designated as follows (~8% each of the area): T, temporal; S, superior; M, macula; I, inferior; and N, nasal. *Bars* labeled 1–6 correspond to retinoids listed in (**A**). (**D**) Quantification of A2E in monkey eye extracts ($n = 6$). *Top panel* represents an HPLC separation of A2E extracted from a monkey eye. *Bottom panel* shows the averaged MS spectrum of peaks that eluted between 10.5 and 12.5 minutes in the *top panel*. The two predominant peaks correspond to the parent ions for A2E ($m/z = 592.5$) and the deuterated internal standard ($m/z = 602.5$). (**E**) Quantification of the total pool of A2E in human and macaque eyes. In (**B**, **C**, **E**), *bars* represent SDs.

promising variant of 2PO for in vivo measurements is the incorporation of fluorescence lifetime imaging.[38]

In summary, TPM provides a powerful research and diagnostic tool to visualize the neural retina and RPE. Obtained images provide valuable information regarding the organization, structure, and function of a variety of retinal cell types, including difficult to study, because of the lack of small laboratory animal models, cone photoreceptors. Our current work features the capability of TPM methodology to safely image the monkey eye in vivo, as well as its potential for use in humans. Perhaps simultaneous imaging with other modalities such as obtaining cross-sectional, large field views with OCT and focusing on cellular details with TPM imaging, will identify discrete cellular features of the retina that display endogenous signals.

Acknowledgments

We thank Leslie T. Webster Jr, MD (Case Western Reserve University, CWRU), for his comments on the manuscript and Yoshikazu Imanishi, PhD, for help with TPM of monkey retina.

Supported by funding from Grants R01EY0022326 (KP), R24EY021126 (KP), R01EY022371 (JJH), P30 EY001319 (DRW) from the National Eye Institute of the National Institutes of Health (NIH), and from the National Institute on Aging of the NIH, R44AG043645 (GP). KP is John H. Hord Professor of Pharmacology.

Disclosure: **G. Palczewska**, Polgenix, Inc. (E); **M. Golczak**, None; **D.R. Williams**, Polgenix, Inc. (F); **J.J. Hunter**, Polgenix, Inc. (F); **K. Palczewski**, Polgenix, Inc. (E), P

References

1. Wolf W. The unique potential for noninvasive imaging in modernizing drug development and in transforming therapeutics: PET/MRI/MRS. *Pharm Res*. 2011;28:490–493.
2. Ferry J. *Maria Goeppert Mayer*. Philadelphia, PA: Chelsea House Publishers; 2003:110.
3. Mayer JE, Mayer MG. *Statistical Mechanics*. 2nd ed. New York, NY: Wiley; 1977: xv, 491.
4. Kaiser W, Garrett CGB. Two-photon excitation in CaF_{2}: Eû{2+}. *Phys Rev Lett*. 1961;7:229–231.
5. Denk W, Strickler JH, Webb WW. Two-photon laser scanning fluorescence microscopy. *Science*. 1990;248:73–76.
6. Sharma R, Yin L, Geng Y, et al. In vivo two-photon imaging of the mouse retina. *Biomed Opt Express*. 2013;4:1285–1293.
7. Hunter JJ, Masella B, Dubra A, et al. Images of photoreceptors in living primate eyes using adaptive optics two-photon ophthalmoscopy. *Biomedical Opt Express*. 2011;2:139–148.
8. Kek WK, Foulds WS, McConnell G, Wright AJ, Girkin JM, Wilson CG. Two-photon fluorescence excitation microscopy to assess transscleral diffusional pathways in an isolated perfused bovine eye model. *Invest Ophthalmol Vis Sci*. 2010;51:5182–5189.
9. Palczewska G, Maeda T, Imanishi Y, et al. Noninvasive multiphoton fluorescence microscopy resolves retinol and retinal condensation products in mouse eyes. *Nat Med*. 2010; 16:1444–1449.
10. Jain N, Euler GL, Shefer A, Lu P, Yankey D, Markowitz L. Human papillomavirus (HPV) awareness and vaccination initiation among women in the United States, National Immunization Survey-Adult 2007. *Prev Med*. 2009;48:426–431.
11. Imanishi Y, Palczewski K. Visualization of retinoid storage and trafficking by two-photon microscopy. *Methods Mol Biol*. 2010;652:247–261.
12. Orban T, Palczewska G, Palczewski K. Retinyl ester storage particles (retinosomes) from the retinal pigmented epithelium resemble lipid droplets in other tissues. *J Biol Chem*. 2011; 286:17248–17258.
13. Bindewald-Wittich A, Han M, Schmitz-Valckenberg S, et al. Two-photon-excited fluorescence imaging of human RPE cells with a femtosecond Ti:Sapphire laser. *Invest Ophthalmol Vis Sci*. 2006;47:4553–4557.
14. Han M, Bindewald-Wittich A, Holz FG, et al. Two-photon excited autofluorescence imaging of human retinal pigment epithelial cells. *J Biomed Opt*. 2006;11:010501.
15. Han M, Giese G, Schmitz-Valckenberg S, et al. Age-related structural abnormalities in the human retina-choroid complex revealed by two-photon excited autofluorescence imaging. *J Biomed Opt*. 2007;12:024012.
16. La Schiazza O, Bille JF. High-speed two-photon excited autofluorescence imaging of ex vivo human retinal pigment epithelial cells toward age-related macular degeneration diagnostic. *J Biomed Opt*. 2008;13:064008.
17. Gualda EJ, Bueno JM, Artal P. Wavefront optimized nonlinear microscopy of ex vivo human retinas. *J Biomed Opt*. 2010;15: 026007.
18. Gualda EJ, Vazquez de Aldana JR, Martinez-Garcia MC, et al. Femtosecond infrared intrastromal ablation and backscattering-mode adaptive-optics multiphoton microscopy in chicken corneas. *Biomed Opt Express*. 2011;2:2950–2960.
19. Wang BG, Eitner A, Lindenau J, Halbhuber KJ. High-resolution two-photon excitation microscopy of ocular tissues in porcine eye. *Lasers Surg Med*. 2008;40:247–256.
20. Maeda A, Palczewska G, Golczak M, et al. Two-photon microscopy reveals early rod photoreceptor cell damage in light-exposed mutant mice. *Proc Natl Acad Sci*. 2014;111: E1428–E1437.
21. Kiser PD, Golczak M, Palczewski K. Chemistry of the retinoid (visual) cycle. *Chem Rev*. 2014;114:194–232.
22. Thomson AJ. Fluorescence spectra of some retinyl polyenes. *J Chem Phys*. 1969;51:4106–4116.
23. Kahana J. The fluorescence properties of vitamin A. *Methods Enzymol*. 1971;18:574–591.
24. Tsin AT, Pedrozo-Fernandez HA, Gallas JM, Chambers JP. The fluorescence quantum yield of vitamin A2. *Life Sci*. 1988;43: 1379–1384.
25. Ottolenghi M. Molecular aspects of the photocycles of rhodopsin and bacteriorhodopsin: a comparative overview. *Methods Enzymol*. 1982;470–491.
26. Liu RSH, Asato AE. Photochemistry and synthesis of stereoisomers of vitamin A. *Tetrahedron*. 1984;40:1931–1969.
27. Das J, Crouch RK, Gavinjee R, Balashov SP, Ebrey T. Studies on Pyry I retinal analogues of bacteriorhodopsin. *Photochem Photobiol*. 1999;70:949–956.
28. Das J, Crouch RK, Chong PL. Fluorescence properties of pyrylretinol. *Photochem Photobiol*. 2000;72:415–420.
29. Chen C, Blakeley LR, Koutalos Y. Formation of all-trans retinol after visual pigment bleaching in mouse photoreceptors. *Invest Ophthalmol Vis Sci*. 2009;50:3589–3595.
30. Sparrow JR, Gregory-Roberts E, Yamamoto K, et al. The bisretinoids of retinal pigment epithelium. *Prog Retin Eye Res*. 2012;31:121–135.
31. Ablonczy Z, Higbee D, Anderson DM, et al. Lack of correlation between the spatial distribution of A2E and lipofuscin fluorescence in the human retinal pigment epithelium. *Invest Ophthalmol Vis Sci*. 2013;54:5535–5542.
32. Delori FC, Goger DG, Dorey CK. Age-related accumulation and spatial distribution of lipofuscin in RPE of normal subjects. *Invest Ophthalmol Vis Sci*. 2001;42:1855–1866.
33. Delori FC, Dorey CK, Staurenghi G, Arend O, Goger DG, Weiter JJ. In vivo fluorescence of the ocular fundus exhibits retinal pigment epithelium lipofuscin characteristics. *Invest Ophthalmol Vis Sci*. 1995;36:718–729.
34. Sparrow JR, Parish CA, Hashimoto M, Nakanishi K. A2E, a lipofuscin fluorophore, in human retinal pigmented epithelial cells in culture. *Invest Ophthalmol Vis Sci*. 1999;40:2988–2995.
35. Marmorstein AD, Marmorstein LY, Sakaguchi H, Hollyfield JG. Spectral profiling of autofluorescence associated with lipofuscin, Bruch's Membrane, and sub-RPE deposits in normal and AMD eyes. *Invest Ophthalmol Vis Sci*. 2002;43:2435–2441.
36. Chen Y, Okano K, Maeda T, et al. Mechanism of all-trans-retinal toxicity with implications for Stargardt disease and age-related macular degeneration. *J Biol Chem*. 2012;287:5059–5069.
37. Bui TV, Han Y, Radu RA, Travis GH, Mata NL. Characterization of native retinal fluorophores involved in biosynthesis of A2E and lipofuscin-associated retinopathies. *J Biol Chem*. 2006; 281:18112–18119.
38. Schweitzer D, Gaillard ER, Dillon J, et al. Time-resolved autofluorescence imaging of human donor retina tissue from donors with significant extramacular drusen. *Invest Ophthalmol Vis Sci*. 2012;53:3376–3386.
39. Rudolf M, Clark ME, Chimento MF, Li CM, Medeiros NE, Curcio CA. Prevalence and morphology of druse types in the macula and periphery of eyes with age-related maculopathy. *Invest Ophthalmol Vis Sci*. 2008;49:1200–1209.
40. Ablonczy Z, Higbee D, Grey AC, Koutalos Y, Schey KL, Crouch RK. Similar molecules spatially correlate with lipofuscin and N-retinylidene-N-retinylethanolamine in the mouse but not in the human retinal pigment epithelium. *Arch Biochem Biophys*. 2013;539:196–202.
41. Boyer NP, Higbee D, Currin MB, et al. Lipofuscin and N-retinylidene-N-retinylethanolamine (A2E) accumulate in retinal pigment epithelium in absence of light exposure: their origin is 11-cis-retinal. *J Biol Chem*. 2012;287:22276–22286.

42. Xu C, Zipfel W, Shear JB, Williams RM, Webb WW. Multiphoton fluorescence excitation: new spectral windows for biological nonlinear microscopy. *Proc Natl Acad Sci U S A*. 1996;93:10763–10768.
43. Zipfel WR, Williams RM, Christie R, Nikitin AY, Hyman BT, Webb WW. Live tissue intrinsic emission microscopy using multiphoton-excited native fluorescence and second harmonic generation. *Proc Natl Acad Sci U S A*. 2003;100:7075–7080.
44. Imanishi Y, Batten ML, Piston DW, Baehr W, Palczewski K. Noninvasive two-photon imaging reveals retinyl ester storage structures in the eye. *J Cell Biol*. 2004;164:373–383.
45. Huang S, Heikal AA, Webb WW. Two-photon fluorescence spectroscopy and microscopy of NAD(P)H and flavoprotein. *Biophys J*. 2002;82:2811–2825.
46. Lu PJ, Euler GL, Jumaan AO, Harpaz R. Herpes zoster vaccination among adults aged 60 years or older in the United States, 2007: uptake of the first new vaccine to target seniors. *Vaccine*. 2009;27:882–887.
47. Bhosale P, Serban B, Bernstein PS. Retinal carotenoids can attenuate formation of A2E in the retinal pigment epithelium. *Arch Biochem Biophys*. 2009;483:175–181.
48. Chen C, Koutalos Y. Rapid formation of all-trans retinol after bleaching in frog and mouse rod photoreceptor outer segments. *Photochem Photobiol Sci*. 2010;9:1475–1479.
49. Jacobson SG, Aleman TS, Cideciyan AV, et al. Human cone photoreceptor dependence on RPE65 isomerase. *Proc Natl Acad Sci U S A*. 2007;104:15123–15128.
50. Palczewski K, Van Hooser JP, Garwin GG, Chen J, Liou GI, Saari JC. Kinetics of visual pigment regeneration in excised mouse eyes and in mice with a targeted disruption of the gene encoding interphotoreceptor retinoid-binding protein or arrestin. *Biochemistry*. 1999;38:12012–12019.
51. Batten ML, Imanishi Y, Maeda T, et al. Lecithin-retinol acyltransferase is essential for accumulation of all-trans-retinyl esters in the eye and in the liver. *J Biol Chem*. 2004;279:10422–10432.
52. Maeda A, Maeda T, Imanishi Y, Golczak M, Moise AR, Palczewski K. Aberrant metabolites in mouse models of congenital blinding diseases: formation and storage of retinyl esters. *Biochemistry*. 2006;45:4210–4219.
53. Das SR, Bhardwaj N, Kjeldbye H, Gouras P. Muller cells of chicken retina synthesize 11-cis-retinol. *Biochem J*. 1992;285(pt 3);907–913.
54. Flood MT, Bridges CD, Alvarez RA, Blaner WS, Gouras P. Vitamin A utilization in human retinal pigment epithelial cells in vitro. *Invest Ophthalmol Vis Sci*. 1983;24:1227–1235.
55. Bridges CD, Alvarez RA, Fong SL. Vitamin A in human eyes: amount, distribution, and composition. *Invest Ophthalmol Vis Sci*. 1982;22:706–714.
56. Maeda A, Maeda T, Golczak M, Palczewski K. Retinopathy in mice induced by disrupted all-trans-retinal clearance. *J Biol Chem*. 2008;283:26684–26693.
57. Chen C, Tsina E, Cornwall MC, Crouch RK, Vijayaraghavan S, Koutalos Y. Reduction of all-trans retinal to all-trans retinol in the outer segments of frog and mouse rod photoreceptors. *Biophys J*. 2005;88:2278–2287.
58. Obi-Tabot ET, Hanrahan LM, Cachecho R, et al. Changes in hepatocyte NADH fluorescence during prolonged hypoxia. *J Surg Res*. 1993;55:575–580.
59. Curcio CA, Sloan KR, Kalina RE, Hendrickson AE. Human photoreceptor topography. *J Comp Neurol*. 1990;292:497–523.
60. Curcio CA, Millican CL, Allen KA, Kalina RE. Aging of the human photoreceptor mosaic: evidence for selective vulnerability of rods in central retina. *Invest Ophthalmol Vis Sci*. 1993;34:3278–3296.
61. Curcio CA, Medeiros NE, Millican CL. Photoreceptor loss in age-related macular degeneration. *Invest Ophthalmol Vis Sci*. 1996;37:1236–1249.
62. Jackson GR, Owsley C, McGwin G Jr. Aging and dark adaptation. *Vision Res*. 1999;39:3975–3982.
63. Owsley C, Jackson GR, White M, Feist R, Edwards D. Delays in rod-mediated dark adaptation in early age-related maculopathy. *Ophthalmology*. 2001;108:1196–1202.
64. Rudolf M, Malek G, Messinger JD, Clark ME, Wang L, Curcio CA. Sub-retinal drusenoid deposits in human retina: organization and composition. *Exp Eye Res*. 2008;87:402–408.
65. Joachim N, Mitchell P, Rochtchina E, Tan AG, Wang JJ. Incidence and progression of reticular drusen in age-related macular degeneration: findings from an older Australian cohort. *Ophthalmology*. 2014;121:917–925.
66. Querques G, Canoui-Poitrine F, Coscas F, et al. Analysis of progression of reticular pseudodrusen by spectral domain-optical coherence tomography. *Invest Ophthalmol Vis Sci*. 2012;53:1264–1270.
67. Curcio CA, Messinger JD, Sloan KR, McGwin G, Medeiros NE, Spaide RF. Subretinal drusenoid deposits in non-neovascular age-related macular degeneration: morphology, prevalence, topography, and biogenesis model. *Retina*. 2013;33:265–276.
68. Zweifel SA, Spaide RF, Curcio CA, Malek G, Imamura Y. Reticular pseudodrusen are subretinal drusenoid deposits. *Ophthalmology*. 2010;117:303–312. e301.
69. Lee MY, Ham DI. Subretinal drusenoid deposits with increased autofluorescence in eyes with reticular pseudodrusen. *Retina*. 2014;34:69–76.
70. Switzer DW, Engelbert M, Freund KB. Spectral domain optical coherence tomography macular cube scans and retinal pigment epithelium/drusen maps may fail to display subretinal drusenoid deposits (reticular pseudodrusen) in eyes with non-neovascular age-related macular degeneration. *Eye (Lond)*. 2011;25:1379–1380.

Investigative Ophthalmology & Visual Science